Intracranial collateralization determines hemodynamic forces for carotid plaque disruption

Brajesh K. Lal, MD,[a] **Kirk W. Beach, PhD, MD,**[b,c] and **David S. Sumner, MD,**[d] *Baltimore, Md; Seattle, Wash; and Springfield, Ill*

Introduction: Percent diameter reduction provides an imperfect assessment of the risk for stroke from carotid atheroembolism. Stroke associated with atherosclerotic carotid stenosis commonly results from plaque disruption brought about by hemodynamic shear stress and Bernoulli forces. The aim of the present study was to predict the effect of incomplete intracranial collateralization through the circle of Willis (COW) on disruptive hemodynamic forces acting on carotid plaques.

Methods: A simple circuit model of the major pathways and collaterals that form and supply the COW was developed. We modeled the intra- and extracranial arterial circuits from standard anatomic references, and the pressure-flow relationships within these conduits from standard fluid mechanics. The pressure drop caused by (laminar and turbulent) flow along the internal carotid artery path was then computed. Carotid circulation to the brain was classified as being with or without collateral connections through the COW, and the extracranial carotid circuit as being with or without severe stenosis. The pressure drop was computed for each scenario. Finally, a linear circuit model was used to compute brain blood flow in the presence/absence of a disconnected COW.

Results: Pressure drop across a carotid artery stenosis increased as the flow rate within the carotid conduit increased. Poststenotic turbulence from a sudden expansion distal to the stenosis resulted in an additional pressure drop. Despite the stenosis, mean brain blood flow was sustained at 4.15 mL/s bilaterally. In the presence of an intact (collateralized) COW, this was achieved by enhanced flow in the contralateral (normal) carotid artery. However, in a disconnected COW, this was achieved by sustained systolic and enhanced diastolic flow through the stenosed artery. For a similar degree of stenosis, flow and velocity across the plaque was much higher when the COW was disconnected compared with an intact COW. Furthermore, the pressure drop across a similar stenosis was significantly higher with a disconnected COW compared with an intact COW.

Conclusions: Incomplete intracranial collateralization through the COW results in increased flow rates and velocities, and therefore large pressure drops across a carotid artery stenosis. This exerts large disruptive shear stress on the plaque compared with patients with an intact COW. Percent diameter reduction provides an inaccurate assessment of risk for atheroembolic stroke. An assessment of carotid flow rates, flow velocities, and the intracranial collateral circulation may add independent information to refine the estimation of stroke risk in patients with asymptomatic carotid atherosclerosis. (J Vasc Surg 2011;54:1461-71.)

Clinical Relevance: Percent carotid narrowing is not an accurate method to assess risk of stroke in patients with carotid stenosis. Stroke from carotid stenosis results from plaque disruption and atheroembolization. We developed a computer model of blood flow through the carotid and intracranial system. We found that high carotid flow rates and velocities, and not tight stenosis alone, resulted in high disruptive shear stress and Bernoulli forces on the plaque. The highest flow rates occurred in individuals without intracranial collateralization. Therefore, carotid flow rates, velocities, and the integrity of the circle of Willis determine risk for carotid plaque disruption, independent of degree of stenosis.

The standard method to assess risk of atheroembolic stroke in patients with carotid stenosis is the degree of arterial narrowing. While asymptomatic patients with stenoses ≥60% do benefit from carotid endarterectomy (CEA), the stroke risk of 11.0% in medically treated patients is only reduced to 5.1% with surgical treatment.[1,2] Over 89% of asymptomatic patients with high-grade stenosis remain stroke-free with medi-

cal therapy alone. Advances in and increased use of medical management for atherosclerosis may have further reduced the risk of stroke from asymptomatic stenosis. For these reasons, there is continuing reluctance among physicians to revascularize asymptomatic patients at the 60% stenosis threshold,[3] and there is an urgent need to identify additional markers to determine the risk for stroke from carotid atherosclerosis.

Stroke from carotid stenosis commonly results from plaque disruption and atheroembolization. Biological factors such as fibrous-cap erosion[4,5] by macrophages,[6-8] hemorrhage,[9] and/or lipid core expansion[10,11] may render the plaque vulnerable to disruption.[12] While magnetic resonance imaging[5] and ultrasound B-mode imaging[13-15] can differentiate symptomatic ruptured from asymptomatic intact plaques, noninvasive markers for plaques that are vulnerable and will rupture in the future remain elusive. Another critical factor in plaque rupture may be hemodynamic shear stress and Bernoulli forces acting on the plaque to mechanically disrupt it. There are several studies that provide evidence for the existence of intraplaque hemorrhage or lipid necrotic cores

within carotid plaques. These are based on histology,[10,11,16-18] ultrasound,[14,19] and magnetic resonance imaging[5,20,21] of the plaques. Large pressure drops across a stenosis can act directly,[22] or can apply shear stress to the plaque manifesting as tensile stress at the proximal edge or shear stress within the plaque,[23-25] to cause plaque disruption; while Bernoulli pressure depression due to high velocities within a stenosis may promote intraplaque hemorrhage.[26]

The aim of the present study was to compute the effect of incomplete intracranial collateralization on disruptive hemodynamic forces acting on a carotid plaque. To accomplish this, a simple circuit model of the major pathways and collaterals that form and supply the circle of Willis (COW) was developed. We modeled the intra- and extracranial arterial circuits from standard anatomic references, and the pressure-flow relationships within these conduits from standard fluid mechanics. This model provided the basis for an examination of the effect of an intact versus a disconnected COW on the hemodynamic forces acting on similar sized carotid bifurcation plaques.

METHODS

Anatomic model. The brain is supplied by three arterial spurs in each hemisphere branching from the COW: the anterior (ACA), middle (MCA), and posterior (PCA) cerebral arteries. The COW acts as a distribution manifold providing a collateralized supply to these cerebral arteries. Three sources provide inflow to the COW manifold: internal carotid arteries (ICA), basilar artery (BA) formed by a confluence of the left and right vertebral arteries (VA), and the ophthalmic artery (OA), which is a branch of each ICA with collateral connections via the external carotid (ECA) to the common carotid artery (CCA) where the ICA originates. Thus, the majority of people have three redundant pathways to the COW, each with a pair of potential inflow sources.

Only half of all people have a complete COW, while 45% have one segment missing or atretic. Five percent have at least two segments missing, thereby disconnecting one distal ICA from the BA and the contralateral ICA. This leads to a non-collateralized (referred to as "disconnected" in this study) COW. Any combination of COW segments may be missing or nonfunctional; for this analysis, missing segments modeled were the ACA and both PCAs. Despite these missing segments, if each ICA supply is normal, then the cerebral hemispheres will remain adequately supplied.

If the COW is complete, brain perfusion is not compromised by a unilateral carotid stenosis because of collateral supply from the contralateral ICA and BA. This collateral compensation allows reduced flow rates to be maintained in the stenotic ICA, which limits the velocity elevation in the stenotic segment. The collateral compensation also maintains arterial pressure in the affected distal ICA and normal perfusion to the ipsilateral eye. However, a disconnected COW plus an ICA stenosis results in pressure reduction in the ipsilateral isolated COW segment. Although collateral supply via the ipsilateral ECA-OA pathway can provide some compensatory flow, perfusion of the ipsilateral cerebral hemisphere is still primarily achieved by the ICA through the stenosis. To sustain

a normal mean flow rate, this ICA will exhibit high intrastenotic velocities. Concurrently, the arterial pressure supplied to the ipsilateral eye will be low and the pulse will be delayed.

Physiological model. We assumed that normal mean blood flow to each cerebral hemisphere was 4.15 mL/s. This was derived from Poels, et al[27]: hemispheric cerebral flow $\sim[(497.4 \text{ mL/min})/(60 \text{ s})]/2 = 4.15 \text{ mL/s}$. The mean flow to each hemisphere includes 6 mL/s flow for 350 ms during systole, plus 3 mL/s flow during diastole. As a result of efficient autoregulation in the brain, this flow to each hemisphere is preserved irrespective of the presence or absence of carotid stenosis, as long as perfusion pressure remains above 60 mm Hg.[28] In our model, none of the stenoses we tested resulted in perfusion pressures below that threshold. Altered flow to the brain via the ECA and VA were not modeled because these collateral pathways contribute limited flow to the brain, and were assumed to be open and connected to the carotid.

Fluid mechanics assumptions. Pressure drop along the carotid artery pathway was computed using methods pioneered by Jean Poiseuille, Henry Darcy, Osborne Reynolds, and Lewis Moody. They are expressed in three equations.

The Hagen-Poiseuille equation for pressure gradient in a tube with laminar Newtonian flow was computed with Equation 1.

$$dp/dL = (128\mu Q)/(\pi D^4) \qquad (1)$$

The turbulent pressure gradient was computed using the friction factor (f) and the Moody diagram, with Equation 2.

$$dp/dL = (8/(2\pi^2))f\rho Q^2/(D^5) \qquad (2)$$

where f increases with tube wall roughness.

Equation 3 for Reynolds number allowed identification of the transition from laminar to turbulent flow and guided the choice between using the Hagen-Poiseuille equation or the Moody friction factor.

$$Re = 4Q/(\pi D\eta) = (\text{intertial forces})/(\text{viscous forces}) \qquad (3)$$

Added to the pressure drop of flow through tubes, the simplified Bernoulli Equation (4) was used to define the maximum pressure drop at the exit of a stenosis into a normal lumen where a sudden expansion allows turbulence to form rather than a streamlined exit. If the transition is streamlined, the kinetic energy is recovered as potential energy (pressure), and there is no Bernoulli pressure drop. If the expansion is sudden, the resulting poststenotic turbulence dissipates kinetic energy as vibrational energy (bruit, murmur, or heat) causing the Bernoulli pressure drop.

$$\delta p = \rho V^2/2 = (8/\pi^2)\rho Q^2/(D^4) \qquad (4)$$

Abbreviations: dp/dL = pressure gradient; δp = pressure drop; Q = volume flow rate; D = lumen diameter; V = blood velocity; μ = viscosity; ρ = density; $\mu/\rho = \eta$ = kinematic viscosity; and π = pi; f = friction factor.

The pressure drop caused by flow along the ICA was computed by adding the equations appropriate to each seg-
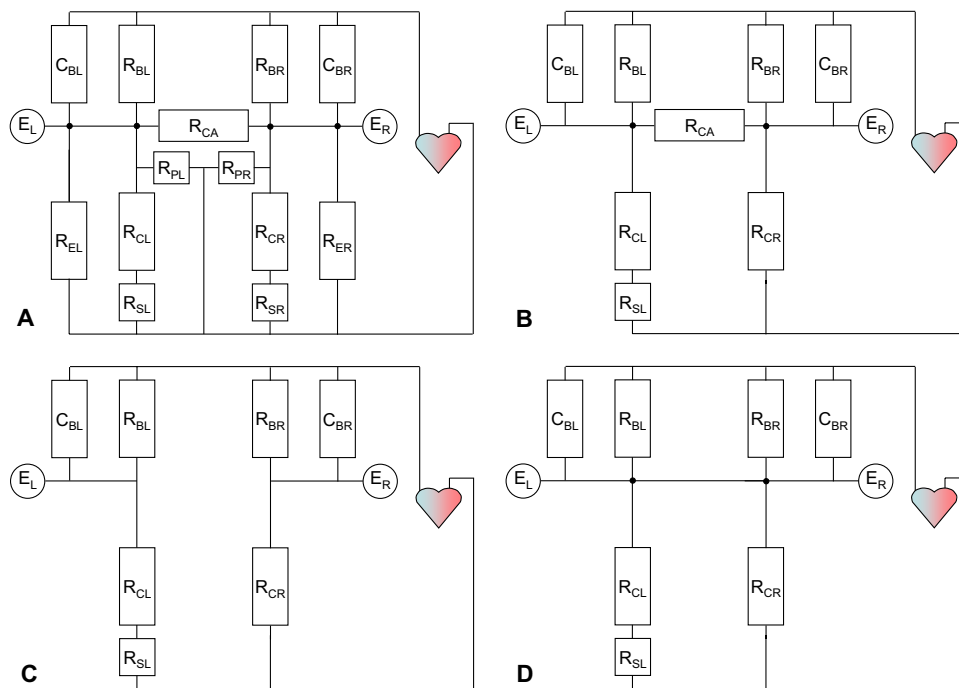
Fig 1. Electrical equivalent circuit of the cerebral circulation. **A**, Detailed circuit of intra- and extracranial circulation. **B**, Abbreviated circuit showing a left carotid artery stenosis and one representative collateral path. **C**, Abbreviated circuit showing a disconnected circle of Willis (COW) with a carotid stenosis. **D**, Abbreviated circuit showing an intact COW. *EL*, Left eye "Test Point"; *ER*, right eye "Test Point." Details of the individual components of the circuit, the anatomical structure they represent, and the values utilized to model a collateralized and disconnected COW are as follows:

Abbreviation	Component	Value for disconnected COW	Value for collateralized COW
C_{BL}	Left brain capacitance	100 mL/mm Hg	100 mL/mm Hg
R_{BL}	Left brain resistance	22.5 mm Hg/(mL/s)	21.0 mm Hg/(mL/s)
R_{BR}	Right brain resistance	15.0 mm Hg/(mL/s)	21.0 mm Hg/(mL/s)
C_{BR}	Right brain capacitance	100 mL/mm Hg	100 mL/mm Hg
R_{CA}	Anterior COW resistance	∞	0
R_{PL}	L post circle resistance	∞	∞
R_{PR}	R post circle resistance	∞	∞
R_{EL}	Left external resistance	∞	∞
R_{CL}	Left ICA resistance	2.5 mm Hg/(mL/s)	2.5 mm Hg/(mL/s)
R_{SL}	Left stenosis resistance	0	0
R_{CR}	Right ICA resistance	2.5 mm Hg/(mL/s)	2.5 mm Hg/(mL/s)
R_{SR}	Right stenosis resistance	7.5 mm Hg/(mL/s)	7.5 mm Hg/(mL/s)
R_{ER}	Right external resistance	∞	∞

ment of the carotid artery conduit for each of the following scenarios: with/without intracranial cross-collateral connections, and with/without extracranial ICA stenosis.

Equivalent circuit model. A linear circuit model was created to represent the cerebral circulation (Fig 1). This consisted of brain components (a capacitor, C, in parallel with a resistor, R), supplied by the carotid component comprising a resistor. The average perfusion pressure difference between the aorta and cerebral veins is ~100 mm Hg and hemispheric flow is ~4 mL/s, so the sum of brain and carotid resistance is 25 mm Hg/(mL/s) (100/4 =

25). These values are derived from true readings.[27] In 982 cases, cerebral blood flow = 497 ± 86.2 mL/min = 4.14 ± 0.7 mL/s (95% confidence interval [CI] 3.44-2.74). So if the mean blood pressure is 100 mm Hg, the 95% CI on cerebral resistance is 36.5 to 18.1 mL/s/mm Hg. Similar results were reported by Fortune et al.[29] The sum of brain and carotid resistance was therefore modeled as 25 mm Hg/(mL/s). In the nonstenotic side, carotid resistance was modeled as 2.5 mm Hg/(mL/s) and the brain as the remaining 22.5 mm Hg/(mL/s); on the stenotic side with a disconnected COW,
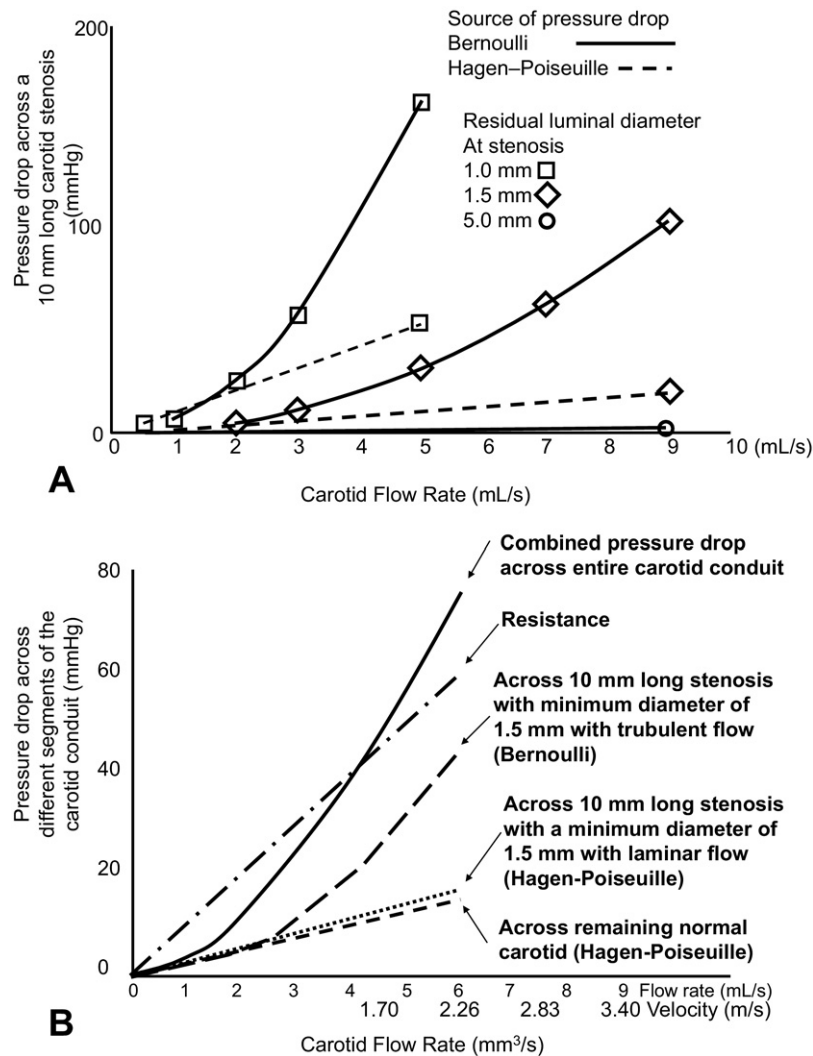
Fig 2. A, Pressure-drops in a 10-mm long carotid stenosis from laminar flow in the stenosis (Hagen-Poiseuille, *dashed lines*) and from turbulence distal to the stenosis (Bernoulli, *solid lines*). Results are shown for different carotid flow rates (typical end-diastolic and peak systolic flow rates are 3 and 6 mL/s), and for different grades of carotid stenoses (normal luminal diameter is assumed = 5.0 mm). **B**, Total pressure-drop across the entire carotid conduit (*bold line*) by adding the individual components (pressure-drop from laminar flow in the stenosis, distal turbulence, and laminar flow in the remaining normal conduit). Derived combined resistance of the conduit = 10mHg/(mL/s).

carotid resistance was modeled as 10 mm Hg/(mL/s) and brain as the remaining 15 mm Hg/(mL/s). Component values were chosen empirically to match the known flow and pressure values listed above. The resulting Equation 5, equating carotid flow with brain storage plus brain flow is:

$$(P(aorta) - P(COW))/(R(carotid))$$
$$= C(brain) \, dp(COW)/dt + P(COW)/R(brain) \quad (5)$$

Using the eye pressure pulsation (P_E) as a measure of the COW pressure, the equation can be rewritten as:

$$(P_A - P_E)/R_C = C_B dP_E/dt + P_E/R_B \quad (5)$$

For the scenario with a complete COW, the equation was solved once using $P_E = P_{ER} = P_{EL}$, $C_B = 2C_{BL} = 2C_{BR}$, $R_C = (R_{CL}*R_{CR})/(R_{CL} + R_{CR})$, and $P_E = P_{ER}/2 = P_{EL}/2$. In the scenario with a disconnected COW with isolated cerebral hemisphere circulation, Equation 5 was solved separately for each side. Thus, carotid blood flow and velocities required to perfuse the brain were assessed in scenarios with and without an intact (collateralized) COW.

RESULTS

Pressure changes with carotid stenosis. An idealized gradual stenosis with a streamlined distal end like a Venturi tube will exhibit Hagen-Poiseuille pressure drop proportional to stenosis length, but will not exhibit additional

Brain blood flow in the presence of a carotid artery stenosis with a complete circle of Willis
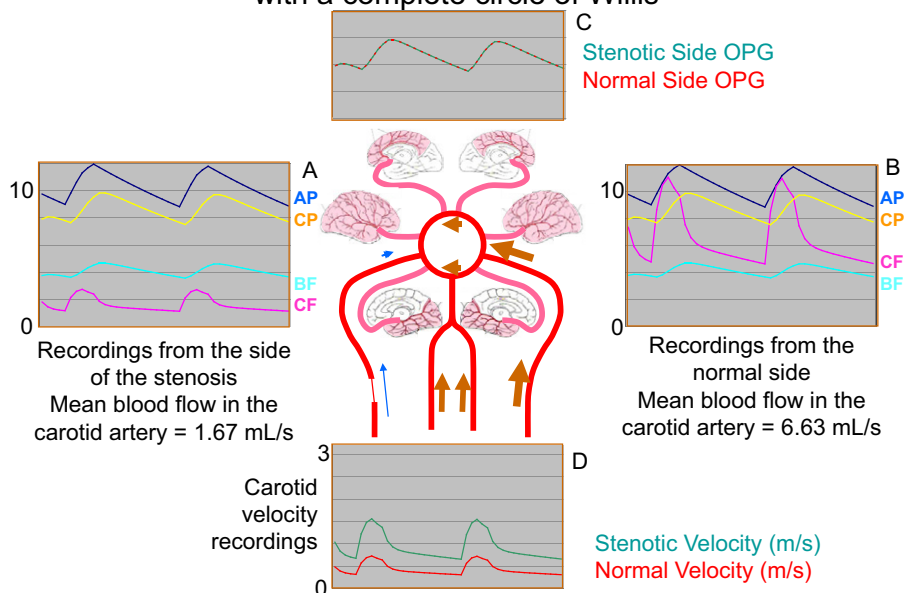
Fig 3. Simulation of brain blood flow in the presence of a carotid artery stenosis and an intact (collateralized) circle of Willis (COW). Results shown are for a 67% stenosis with a residual diameter of 1.5 mm and with poststenotic turbulence (see *center panel*). The aortic (AP, cm Hg) and CP (cm Hg) remain identical in both, the stenotic **(A)** and the normal **(B)** side. Of note the mean brain BF (mL/s) is sustained despite the stenosis but peak systolic CF (mL/s) is blunted. Oculoplethysmography (*OPG*) recordings **(C)** demonstrate no difference between the two sides. Carotid velocities **(D)** are appropriately elevated on the stenotic side (1.5 m/s) compared with the normal side (0.75 m/s). *AP,* Aortic pressure (cm/Hg); *BF,* brain blood flow (mL/s); *CF,* carotid blood flow (mL/s); *CP,* COW pressure (cm/Hg). *Thickness of arrows* indicate amount of blood flow.

Bernoulli pressure drop since there will be no poststenotic turbulence. Conversely, if the stenosis ends abruptly or irregularly, we anticipate a Hagen-Poiseuille pressure drop contributed by the stenosis, followed by additional Bernoulli pressure drop from poststenotic turbulence. The sum of these provides the total pressure drop at the distal ICA and reflects the most common clinical presentation.

We first computed individual components of pressure drops at systolic and diastolic flow rates assuming a 10-mm long unilateral ICA stenosis. Fig 2, *A* demonstrates the results of our analyses for pressure drops contributed by the stenosis (Hagen-Poiseuille) and by the distal turbulence (Bernoulli), for different grades of stenoses, and for typical flow rates within the carotid artery. These represent the pressures encountered at the plaque. For these computations, we assumed: baseline carotid diameter = 5.0 mm; physiological end-diastolic flow = 3mL/s; and physiological peak systolic flow = 6 mL/s.[30]

We found that pressure drop increased as the flow rate within the carotid artery increased. Pressure drop from the stenosis alone (Hagen-Poiseuille) was small when the residual luminal diameter at the ICA stenosis was >1 mm. For instance, at a peak systolic flow rate of 6 mL/s, the pressure drop was only 12 mm Hg for a 10-mm long stenosis with residual luminal diameter of 1.5 mm (Fig 2, *A*). When

additional poststenotic turbulence (Bernoulli) was modeled, then the pressure dropped (Fig 2, *A*) an additional 46 mm Hg, and the total systolic pressure drop from this stenosis became 58 mm Hg. Thus, a 70% ICA stenosis (residual lumen of 1.5 mm), resulted in a severe (58 mm Hg) or mild (12 mm Hg) pressure drop depending on the shape of the distal end of the plaque.

The sum of pressure drop (1) across the plaque (Hagen-Poiseuille plus Bernoulli) and (2) across the distal normal arterial lumen (Hagen-Poiseuille) provides the total pressure drop experienced across the entire carotid artery conduit. In Fig 2, *B*, the components of pressure drop in successive segments of the carotid conduit were added together to provide a total result (Fig 2, *B*, *bold line*).

Flow changes. In the combined pressure/flow diagram (Fig 2, *B*), a sloped dotted line was added (labeled Resistance) denoting stenotic lumen resistance = 10 mm Hg/(mL/s) which is an approximation of the true pressure/flow line. When the pressure/flow relationship is linear with a zero intercept, the line can be represented as a "resistance," and linear circuit theory can be applied to the complex arterial network supplying the brain. In our model, the circuit was simplified to assess brain and carotid blood flow in the presence/absence of carotid stenosis and in the presence/absence of a disconnected COW (Figs 3 and 4).

Brain blood flow in the presence of a carotid artery stenosis with a disconnected circle of Willis
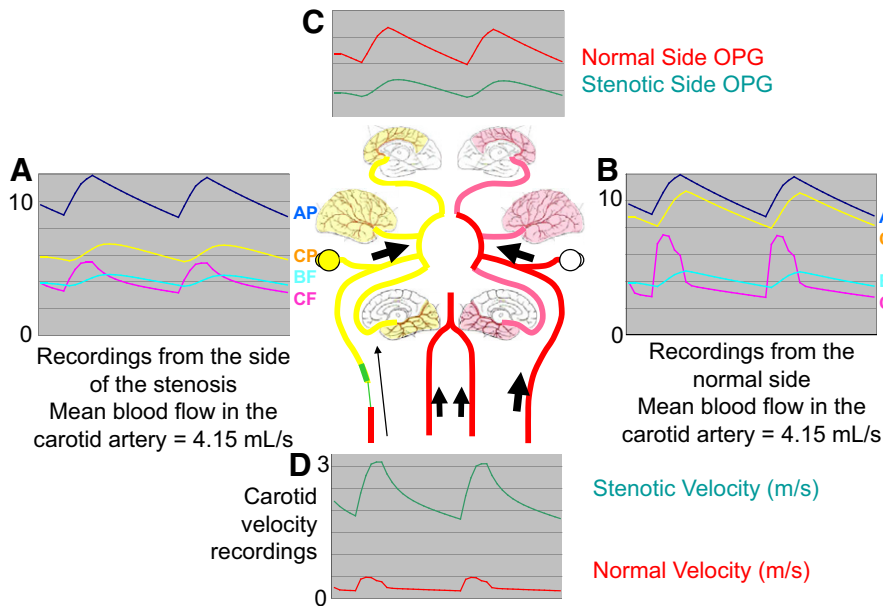

Fig 4. Simulation of brain blood flow in the presence of a carotid artery stenosis and a disconnected circle of Willis (COW). Results shown are for a 67% stenosis with a residual diameter of 1.5 mm and with poststenotic turbulence (see *center panel*). The CP (cm Hg) is significantly reduced on the side with a carotid stenosis **(A)** compared with the normal side **(B)**. Mean brain BF (mL/s) is sustained on the stenosed side through an elevation of diastolic flow and prolonged systolic flow. The oculoplethysmography (*OPG*) recordings **(C)** demonstrate a delay in peak systole with low amplitude on the side with a stenosis. Also of note, carotid velocities **(D)** were significantly higher on the stenotic side in this scenario (3.2 m/s), compared with the normal side (0.5 m/s). *AP,* Aortic pressure (cm/Hg); *BF,* brain blood flow (mL/s); *CF,* carotid blood flow (mL/s); *CP,* COW pressure (cm/Hg). *Thickness of arrows* indicate amount of blood flow.

In a stenosis with a complete (collateralized) COW, circuit simulation of each hemisphere separately (Fig 3) showed that mean brain blood flow was sustained by increasing the flow through the contralateral (normal) carotid artery. On that side, the ratio of peak systolic flow (PSQ) to end diastolic flow (EDQ) was 11.02/4.62 = 2.39, and mean flow was 6.63 mL/s. On the stenotic side the ratio was 2.76/1.15 = 2.40 and mean flow in the carotid was only 1.67 mL/s.

In a symmetrically disconnected (non-collateralized) COW, each ICA had to supply its own cerebral hemisphere (Fig 4). Mean brain flow could not be sustained on the stenosed side by increasing flow through the contralateral side, and each ICA had to maintain a flow rate = 4.15 mL/s on its own. Circuit simulation showed that this was achieved by a ratio of peak systolic flow to end diastolic flow on the stenosed side of 5.48/3.19 = 1.72, and on the contralateral side of 7.48/2.80 = 2.67. Therefore, mean flow was sustained in the stenosed carotid conduit (at 4.15 mL/s) by increasing diastolic flow and by spreading systolic flow over a longer time period. Peak flow in the stenotic carotid occurred 250 ms after the onset of systole, significantly later than the 100 ms delay on the normal side. These findings should prompt one to consider the possibility of
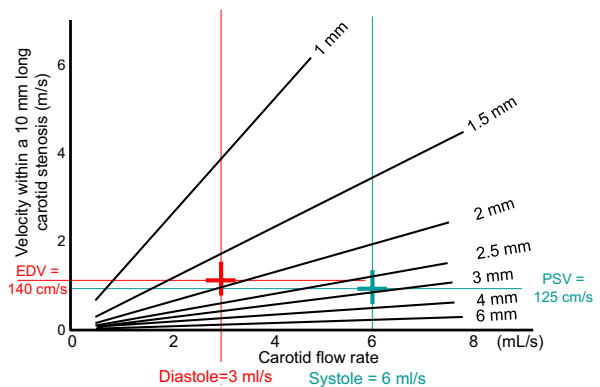

Fig 5. Blood flow velocity across a carotid stenosis is influenced by the carotid flow rate and by the severity of stenosis. Assuming a mean normal internal carotid artery (ICA) diameter of 5.0 mm, a residual luminal diameter of 2.5 mm will correspond to a 50% stenosis and a residual diameter of 1.5 mm will correspond to a 70% stenosis. The changes in carotid velocity with increasing flow rates are plotted for individual degrees of carotid artery stenosis. The residual luminal diameter is listed against its corresponding plot in the graph.

Table. Predicted hemodynamic parameters in the ipsilateral (67% stenosis) and contralateral (normal) internal carotid artery with a collateralized or disconnected COW

Parameter	Ipsilateral ICA		Contralateral ICA	
	Collateralized COW	*Disconnected COW*	*Collateralized COW*	*Disconnected COW*
Peak systolic velocity	1.56 m/s	3.10 m/s	0.73 m/s	0.49 m/s
End diastolic velocity	0.65 m/s	1.81 m/s	0.30 m/s	0.18 m/s
Peak delay	150 ms	250 ms	150 ms	100 ms
Peak systolic flow	2.76 mL/s	5.48 mL/s	11.02 mL/s	7.48 mL/s
End diastolic flow	1.15 mL/s	3.19 mL/s	4.62 mL/s	2.80 mL/s
Mean flow	1.67 mL/s	4.15 mL/s	6.63 mL/s	4.15 mL/s
Systolic/diastolic ratio	2.40	1.72	2.39	2.67

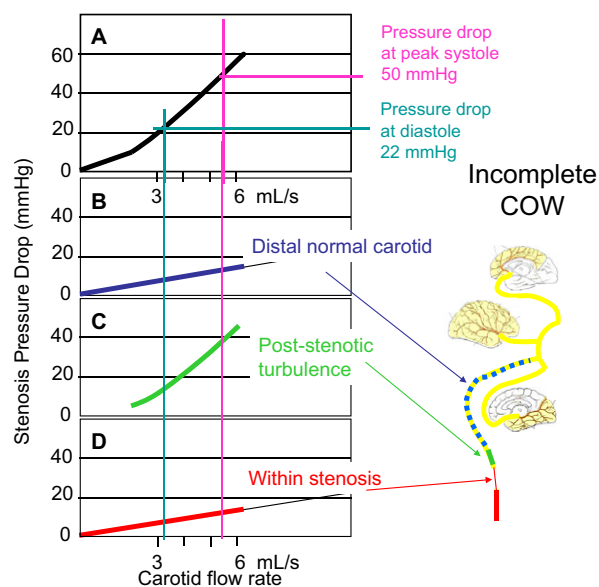*COW*, Circle of Willis; *ICA*, internal carotid artery.

Fig 6. Pressure drop across a 67% diameter-reducing carotid artery stenosis in the presence of an intact circle of Willis (*COW*). **A** depicts final pressure drop after summing the pressure drops across the distal normal carotid segment (laminar flow, Poiseuille, **B**), at the distal end of the stenosed segment (turbulent flow, Bernoulli, **C**), and across the stenosed segment (laminar flow, Poiseuille, **D**). The corresponding pressure drops at peak systolic and peak diastolic flows are shown on **A**.

isolated intracranial anatomy. There was a corresponding delay in oculoplethysmography (OPG) recordings and a larger rise in carotid velocities compared with the collateralized case (Fig 3, *C* and *D*).

Velocity changes. The relationship between ICA luminal diameter (ie, stenosis) and velocity is affected by the arterial flow rate. Velocity within a stenosis was plotted against carotid flow rates with increasing stenoses (Fig 5). Effects of turbulence, helical or parabolic flow, and the Doppler angle were not included. Velocities obtained from this model were consistent with clinical reports in the literature, thereby validating our simple model.

Arterial velocities were also affected by the status of COW collateralization. We modeled the two scenarios of an intact versus a disconnected COW using the same angiographic degree of stenosis (67%) in both cases (Table). With a disconnected COW, a 67% stenosis demonstrated an end diastolic velocity that exceeded the traditional criteria (1.4 m/s) for severe stenosis (≥70%) (Fig 4, *D*). The same 67% stenosis demonstrated a diastolic velocity below that criterion when the COW was intact (Fig 3, *D*).

Pressure changes with disconnected COW. We first modeled a unilateral 10-mm long 67% ICA stenosis in the presence of a disconnected COW. The mean flow through each carotid artery was 4.15 mL/s, peak systolic flow was 6 mL/s for a short period of time, and diastolic flow was 3 mL/s for a longer period. Fig 6 shows the pressure drop across the normal distal conduit (Fig 6, *B*), from poststenotic turbulence (Fig 6, *C*), and across the stenotic segment (Fig 6, *D*), respectively. Fig 6, *A* depicts the sum of the pressure drops from the stenosis and the poststenotic turbulence (ie, the total pressure drop that the plaque would be subjected to as a function of flow rate). At the carotid flow rates existing in patients with a disconnected COW, the plaque experienced a pressure drop of 50 mm Hg during systole and 22 mm Hg in diastole.

We next modeled an identical stenosis (67%, 10-mm long) in a patient with an intact COW (Fig 7). The normal (contralateral, non-stenosed) carotid artery carried 80% of total flow to the brain, and provided 60% of contralateral hemispheric blood supply. In contrast to patients with a disconnected COW, the same plaque in an intact system would only be subject to a pressure drop of 15 mm Hg in systole and 10 mm Hg in diastole (Fig 7).

OPG waveform changes. In the presence of a carotid stenosis, the degree of intracranial collateralization affects the blood supply to the periorbital region. OPG displays a tracing of each eye diameter waveform, (Figs 3, *C* and 4, *C*). These graphs show that an uncollateralized stenosis is associated with a significant and measurable delay in the systolic peak.
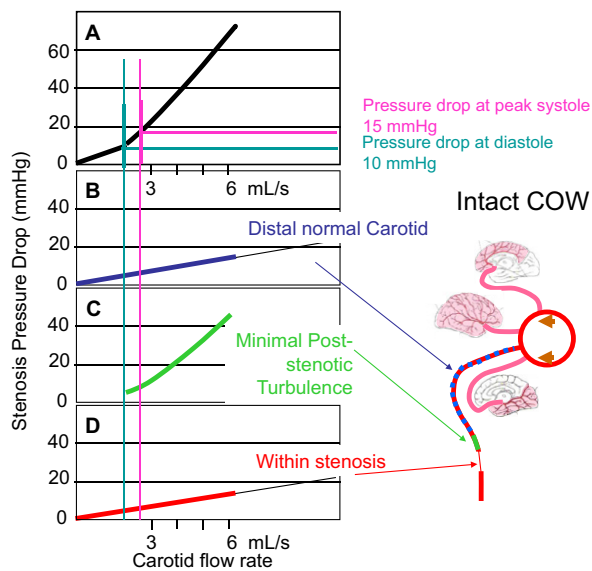
Fig 7. Pressure drop across a 67% diameter-reducing carotid artery stenosis in the presence of a disconnected circle of Willis (*COW*). **A** depicts final pressure drops after summing the pressure drops across the distal normal carotid segment (laminar flow, Poiseuille, **B**), at the distal end of the stenosed segment (turbulent flow, Bernoulli, **C**), and across the stenosed segment (laminar flow, Poiseuille, **D**). The corresponding pressure drops at peak systolic and peak diastolic flows are shown on **A**.

DISCUSSION

Disruptive hemodynamic forces on carotid atherosclerotic plaques are increased when intracranial arterial collateralization through the COW is incomplete. In the absence of COW collateralization, the mean carotid flow rate must be sustained, even if this results in a significant trans-stenotic pressure drop (Figs 4 and 6) thereby generating severe stress (Fig 8). Large pressure drops across a stenosis can act directly,[22] or can apply shear stress to the plaque.[23-25,31] If the plaque core were liquid (and therefore unable to withstand shear stress) then the proximal cap would relieve that strain by rupturing. In contrast, the same plaque in a collateralized system is subject to lower flow rates and lower pressure drops (Figs 3 and 7), thereby rendering the plaque less vulnerable to rupture (Fig 8). Percent diameter reduction has been used for over half a century as the only scale for estimating the risk of stroke from carotid plaques. Our analysis suggests that an assessment of the intracranial collateral circulation may add independent information to refine the estimation of stroke risk.

Several techniques can assess the physiological integrity of the COW. In this analysis, we modeled OPG since it is well recognized that a delay in the systolic peak in its waveform indicates uncollateralized carotid stenosis.[32] OPG simultaneously measures bilateral ocular and external carotid pulses. Pulse delays reliably reflect reduced pressure in the internal and/or external carotid arteries, respectively. The pulse delay does not occur if the COW is intact and provides

collateral flow. Computed tomography, magnetic resonance angiography,[33] or transcranial Doppler (TCD) may also ascertain the anatomic integrity of the COW. Of these, TCD would potentially provide the most cost-effective assessment in a clinical environment.

Carotid auscultation for bruits has been a traditional yet inaccurate method of screening for carotid stenosis. Although ICA bruits have low specificity for carotid stenosis, our results indicate that they may identify plaques most likely to rupture. Carotid bruits indicate poststenotic turbulence. According to our analysis (Fig 6), once a diagnosis of carotid stenosis has been confirmed, then the presence of a bruit could indicate a non-collateralized COW. In one report, OPG pulse delay with an associated carotid bruit carried a 17% risk of stroke with CEA compared with a 1% risk in the absence of these findings.[34]

The relationship between percent carotid stenosis and risk for plaque disruption is modest at best. We found that increasing carotid flow rates resulted in progressively larger pressure drops (Figs 2, B and 6; Hagen-Poiseuille plus Bernoulli), generating larger disruptive hydraulic shear forces at the distal end of the plaque. Therefore, carotid flow rate is an additional factor that must be considered in assessing the risk for stroke.

If flow rate influences risk for plaque rupture, then any situation that increases carotid flow rate and intrastenotic velocities should also predispose to an atheroembolic stroke. In atrial fibrillation (AF), the beat following a prolonged RR interval (in an electrocardiogram) is associated with increased carotid flow rate and velocity because of the uncompensated excess peak systolic pressure. Of note, approximately 15% of patients with AF will experience a stroke during their life-time.[35] All ischemic strokes in these patients are not necessarily cardiogenic. Fifty percent of patients with AF have detectable carotid stenosis, and 11% to 24% have stenoses >50%.[36,37] While it is difficult to differentiate the etiology of ischemic stroke when two risk factors coexist, in various reports 5% to 20% of strokes in patients with AF have been attributed to atheroembolism from their carotid plaques.[38,39] In this subpopulation of patients, strokes tend to occur more frequently and are more extensive compared with those with AF alone. Our results provide a potential explanation for the pathogenesis of atheroembolic stroke in patients with coexistent AF and carotid plaques.

Patients with sleep apnea have a higher rate of stroke compared with normal individuals. This risk has been attributed to the increased incidence of hypertension, heart disease, and coagulopathy found in these patients.[40,41] However, sleep apnea is also associated with hypercapnia and consequent intracranial vasodilation, which is associated with an increase in carotid artery flow rates. While the incidence of carotid plaques in sleep apnea patients is not known, our analysis indicates that plaques in these patients would be subject to increased hemodynamic disruptive forces, thereby providing a potential explanation for the increased stroke rates in these patients.
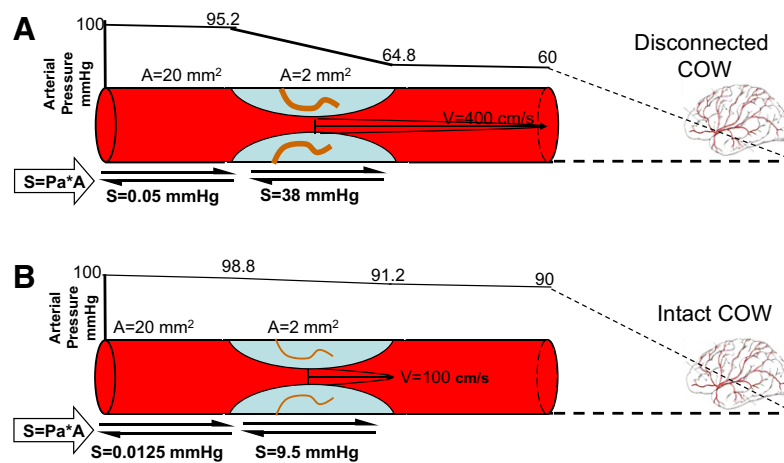
Fig 8. Disruptive hemodynamic forces on extracranial carotid atherosclerotic plaques are increased when intracranial arterial collateralization through the COW is incomplete. **A,** In the absence of COW collateralization, the mean carotid flow rate must be sustained, even if this results in a significant trans-stenotic pressure drop generating severe stress that could result in plaque rupture. **B,** In contrast, the same plaque in a collateralized system is subject to lower flow rates, lower velocities, and lower pressure drops, thereby rendering the plaque less vulnerable to rupture. Intraplaque vasa-vasorum are shown drawn in *brown. A,* Cross-sectional area of arterial lumen; *COW,* circle of Willis; *Pa,* arterial pressure; *S,* shear; *V,* peak systolic velocity.

It is well known that a stenosis or occlusion in one ICA may elevate velocities in the opposite ICA and, in some instances, the elevation may be high enough to falsely suggest that a stenosis is present.[42-44] This has prompted vascular laboratories to modify their threshold velocity criteria for stenosis assessment when disease is present in the opposite artery. Our results confirm these clinical findings (Table), thereby validating our mathematical model.

Relative increases in shear stress of 170% have correlated with an increased risk of plaque rupture.[45] Li et al have reported that wall shear stress (WSS) rises with increasing stenosis severity and associated peak systolic velocities (PSV) within the carotid artery.[46] They found that a PSV of 1.47 m/s corresponded to a maximum WSS of 40 Pa; and a PSV of 3.2 m/s corresponded to an increased WSS of 220 Pa. Our own modeling predicts a PSV of 3.1 m/s in a carotid stenosis of 67% when associated with a disconnected COW. This corresponds to an extremely elevated shear stress, well beyond the threshold that predicts a high risk of plaque rupture.[45]

Flow rate and velocity elevations in the carotid artery varied with the integrity of intracranial collateralization (Table), and we found that a disconnected COW caused a significantly higher PSV in an ICA with a 67% stenosis (3.10 m/s) compared with the PSV in an ICA with an intact COW (1.56 m/s). Conversely, a disconnected COW was not associated with a compensatory rise in PSV in the opposite ICA (0.49 m/s), while a compensatory rise in velocity did occur when the COW was intact (0.73 m/s). This may explain why carotid velocities do not perfectly correlate with angiographic stenosis,[47] despite adjustments for contralateral stenoses.[44] The possibility of a disconnected COW must therefore be entertained when interpreting velocities for assigning degree of carotid stenosis.

Limitations. Our model does not account for variability in pressure drops incurred by carotid lesions with irregular surfaces and mixed geometry. The variability is infinite and thus impossible to account for in any model. However, we have placed some simplified boundaries on the relationship between pressure drop and flow. The exact relationship between measured Doppler velocity and flow rate will be affected by the stenosis morphology, but it will not change the overall concept that collateralization through the COW affects carotid flow and forces on the plaque. We have not accounted for the VA or the ECA as potential collaterals to the COW. We believe that for the purposes of establishing the importance of collateralization through the COW, and how it may affect the relationship between Doppler velocity and anatomic stenosis measurement, modeling for the VA or ECA may be useful, but not critical. Our findings indicate an important role for a disconnected COW in enhancing risk of atheroembolic stroke from carotid stenosis. However, a disconnected COW also creates an isolated hemisphere that may present an increased risk (as yet untested and unproven) for perioperative stroke associated with CEA. As vascular surgeons, we have progressively improved our techniques for identifying cerebral hypoperfusion during surgery (eg, stump pressure, awake surgery, or neural monitoring), and taking actions to prevent ischemia (selective shunting). For those that do not utilize these techniques, mandatory shunting is an alternative. Carotid artery stenting may be another alternative in such situations, since the ICA is occluded for only a few seconds during the procedure. We would argue that foreknowledge of a disconnected COW will enhance outcomes of carotid revascularization since it will forewarn surgeons about these risks.

CONCLUSIONS

We have developed a simple model of blood flow through the carotid system that enhances understanding of a complex network of vessels. Individuals with high carotid flow rates and flow velocities, and not those with a tight angiographic carotid artery stenosis alone, (although these groups may overlap) are at a high risk for carotid plaque disruption and atheroembolization. High carotid flow rates and flow velocities are encountered in individuals without intracranial collateralization through the COW. Additional subgroups of patients with episodic increases in carotid artery flow rates and velocities include those with sleep apnea or cardiac arrhythmia, and may have an enhanced risk for stroke. We suggest that carotid flow rates, flow velocities, and the integrity of the COW are key determinants of the risk for carotid plaque disruption that must be evaluated in patients with asymptomatic carotid plaques. Clinical studies will be required to validate these findings.

AUTHOR CONTRIBUTIONS

Conception and design: BL
Analysis and interpretation: BL, KB, DS
Data collection: BL, KB
Writing the article: BL
Critical revision of the article: BL, KB, DS
Final approval of the article: BL, KB, DS
Statistical analysis: BL, KB
Obtained funding: BL
Overall responsibility: BL

REFERENCES

1. Executive Committee for the Asymptomatic Carotid Atherosclerosis Study. Endarterectomy for asymptomatic carotid artery stenosis. JAMA 1995;273:1421-8.
2. Barnett HJ, Meldrum HE, Eliasziw M. The dilemma of surgical treatment for patients with asymptomatic carotid disease. Ann Intern Med 1995;123:723-5.
3. Klein A, Solomon CG, Hamel MB. Clinical decisions. Management of carotid stenosis--polling results. N Engl J Med 2008;358:e23.
4. Kilpatrick D, Goudet C, Sakaguchi Y, Bassiouny HS, Glagov S, Vito R. Effect of plaque composition on fibrous cap stress in carotid endarterectomy specimens. J Biomech Eng 2001;123:635-8.
5. Hatsukami TS, Ross R, Polissar NL, Yuan C. Visualization of fibrous cap thickness and rupture in human atherosclerotic carotid plaque in vivo with high-resolution magnetic resonance imaging. Circulation 2000;102:959-64.
6. Li W, Kornmark L, Jonasson L, Forssell C, Yuan XM. Cathepsin L is significantly associated with apoptosis and plaque destabilization in human atherosclerosis. Atherosclerosis 2009;202:92-102.
7. Howarth S, Li ZY, Trivedi RA, U-King-Im JM, Graves MJ, Kirkpatrick PJ, et al. Correlation of macrophage location and plaque stress distribution using USPIO-enhanced MRI in a patient with symptomatic severe carotid stenosis: a new insight into risk stratification. Br J Neurosurg 2007;21:396-8.
8. Nikkari ST, O'Brien KD, Ferguson M, Hatsukami T, Welgus HG, Alpers CE, et al. Interstitial collagenase (MMP-1) expression in human carotid atherosclerosis. Circulation 1995;92:1393-8.
9. Avril G, Batt M, Guidoin R, Marois M, Hassen-Khodja R, Daune B, et al. Carotid endarterectomy plaques: correlations of clinical and anatomic findings. Ann Vasc Surg 1991;5:50-4.
10. Bassiouny HS, Sakaguchi Y, Mikucki SA, McKinsey JF, Piano G, Gewertz BL, et al. Juxtalumenal location of plaque necrosis and

11. neoformation in symptomatic carotid stenosis. J Vasc Surg 1997;26:585-94.
11. Falk E. Why do plaques rupture? Circulation 1992;86(6 Suppl): III30-42.
12. Barnett HJ, Eliasziw M, Meldrum H. Plaque morphology as a risk factor for stroke. JAMA 2000;284:177.
13. Lal BK, Hobson RW 2nd, Hameed M, Pappas PJ, Padberg FT Jr, Jamil Z, et al. Noninvasive identification of the unstable carotid plaque. Ann Vasc Surg 2006;20:167-74.
14. Lal BK, Hobson RW 2nd, Pappas PJ, Kubicka R, Hameed M, Chakhtoura EY, et al. Pixel distribution analysis of B-mode ultrasound scan images predicts histologic features of atherosclerotic carotid plaques. J Vasc Surg 2002;35:1210-7.
15. Biasi GM, Froio A, Diethrich EB, Deleo G, Galimberti S, Mingazzini P, et al. Carotid plaque echolucency increases the risk of stroke in carotid stenting: the Imaging in Carotid angioplasty and Risk of Stroke (ICAROS) study. Circulation 2004;110:756-62.
16. Hiyama T, Tanaka T, Endo S, Komine K, Kudo T, Kobayashi H, et al. Angiogenesis in atherosclerotic plaque obtained from carotid endarterectomy: association between symptomatology and plaque morphology. Neurol Med Chir (Tokyo); 2010;50:1056-61.
17. Redgrave JN, Lovett JK, Gallagher PJ, Rothwell PM. Histological assessment of 526 symptomatic carotid plaques in relation to the nature and timing of ischemic symptoms: the Oxford Plaque Study. Circulation 2006;113:2320-8.
18. Stary HC. Natural history and histological classification of atherosclerotic lesions: an update. Arterioscler Thromb Vasc Biol 2000;20: 1177-8.
19. Geroulakos G, Hobson RW, Nicolaides A. Ultrasonographic carotid plaque morphology in predicting stroke risk. Br J Surg 1996;83:582-7.
20. Sadat U, Teng Z, Young VE, Li ZY, Gillard JH. Utility of magnetic resonance imaging-based finite element analysis for the biomechanical stress analysis of hemorrhagic and non-hemorrhagic carotid plaques. Circ J 2011;75:884-9.
21. Zhao XQ, Phan BA, Chu B, Bray F, Moore AB, Polissar NL, et al. Testing the hypothesis of atherosclerotic plaque lipid depletion during lipid therapy by magnetic resonance imaging: study design of Carotid Plaque Composition Study. Am Heart J 2007;154:239-46.
22. Li ZY, Taviani V, Gillard JH. The impact of wall shear stress and pressure drop on the stability of the atherosclerotic plaque. Conf Proc IEEE Eng Med Biol Soc 2008;2008:1373-6.
23. Fukumoto Y, Hiro T, Fujii T, Hashimoto G, Fujimura T, Yamada J, et al. Localized elevation of shear stress is related to coronary plaque rupture: a 3-dimensional intravascular ultrasound study with in-vivo color mapping of shear stress distribution. J Am Coll Cardiol 2008;51: 645-50.
24. Xue YJ, Gao PY, Duan Q, Lin Y, Dai CB. Preliminary study of hemodynamic distribution in patient-specific stenotic carotid bifurcation by image-based computational fluid dynamics. Acta Radiol 2008; 49:558-65.
25. Li ZY, Tang T, U-King-Im J, Graves M, Sutcliffe M, Gillard JH. Assessment of carotid plaque vulnerability using structural and geometrical determinants. Circ J 2008;72:1092-9.
26. Beach KW, Hatsukami T, Detmer PR, Primozich JF, Ferguson MS, Gordon D, et al. Carotid artery intraplaque hemorrhage and stenotic velocity. Stroke 1993;24:314-9.
27. Poels MM, Ikram MA, Vernooij MW, Krestin GP, Hofman A, Niessen WJ, et al. Total cerebral blood flow in relation to cognitive function: the Rotterdam Scan Study. J Cereb Blood Flow Metab 2008;28:1652-5.
28. Spencer MP, Thomas GI, Moehring MA. Relation between middle cerebral artery blood flow velocity and stump pressure during carotid endarterectomy. Stroke 1992;23:1439-45.
29. Fortune JB, Bock D, Kupinski AM, Stratton HH, Shah DM, Feustel PJ. Human cerebrovascular response to oxygen and carbon dioxide as determined by internal carotid artery duplex scanning. J Trauma 1992; 32:618-27; discussion:627-8.
30. Bartlett ES, Walters TD, Symons SP, Fox AJ. Quantification of carotid stenosis on CT angiography. AJNR Am J Neuroradiol 2006;27:13-9.

31. Tang D, Yang C, Kobayashi S, Ku DN. Effect of a lipid pool on stress/strain distributions in stenotic arteries: 3-D fluid-structure interactions (FSI) models. J Biomech Eng 2004;126:363-70.

32. McRae LP, Cadwallader JA 3rd, Kartchner MM. Oculoplethysmography and carotid phonoangiography for the noninvasive detection of extracranial carotid occlusive disease. Med Instrum 1979;13:87-91.

33. Brisman JL, Pile-Spellman J, Konstas AA. Clinical utility of quantitative magnetic resonance angiography in the assessment of the underlying pathophysiology in a variety of cerebrovascular disorders [published online ahead of print February 10, 2011]. Eur J Radiol doi:10.1016/j.ejrad.2010.12.079.

34. Kartchner MM, McRae LP. Carotid occlusive disease as a risk factor in major cardiovascular surgery. Arch Surg 1982;117:1086-8.

35. Hart RG, Halperin JL. Atrial fibrillation and thromboembolism: a decade of progress in stroke prevention. Ann Intern Med 1999;131:688-95.

36. Kanter MC, Tegeler CH, Pearce LA, Weinberger J, Feinberg WM, Anderson DC, et al. Carotid stenosis in patients with atrial fibrillation. Prevalence, risk factors, and relationship to stroke in the Stroke Prevention in Atrial Fibrillation Study. Arch Intern Med 1994;154:1372-7.

37. van Latum JC, Koudstaal PJ, Venables GS, van Gijn J, Kappelle LJ, Algra A. Predictors of major vascular events in patients with a transient ischemic attack or minor ischemic stroke and with nonrheumatic atrial fibrillation. European Atrial Fibrillation Trial (EAFT) Study Group. Stroke 1995;26:801-6.

38. Chang YJ, Ryu SJ, Lin SK. Carotid artery stenosis in ischemic stroke patients with nonvalvular atrial fibrillation. Cerebrovasc Dis 2002;13:16-20.

39. Hart RG, Pearce LA, Miller VT, Anderson DC, Rothrock JF, Albers GW, et al. Cardioembolic vs. noncardioembolic strokes in atrial fibrillation: frequency and effect of antithrombotic agents in the stroke prevention in atrial fibrillation studies. Cerebrovasc Dis 2000;10:39-43.

40. Arzt M, Young T, Finn L, Skatrud JB, Bradley TD. Association of sleep-disordered breathing and the occurrence of stroke. Am J Respir Crit Care Med 2005;172:1447-51.

41. Somers VK, White DP, Amin R, Abraham WT, Costa F, Culebras A, et al; American Heart Association Council for High Blood Pressure Research Professional Education Committee, Council on Clinical Cardiology; American Heart Association Stroke Council; American Heart Association Council on Cardiovascular Nursing; American College of Cardiology Foundation. Sleep apnea and cardiovascular disease: an American Heart Association/American College of Cardiology Foundation Scientific Statement from the American Heart Association Council for High Blood Pressure Research Professional Education Committee, Council on Clinical Cardiology, Stroke Council and Council on Cardiovascular Nursing. In collaboration with the National Heart, Lung, and Blood Institute National Center on Sleep Disorders Research (National Institutes of Health). Circulation 2008;118:1080-111.

42. AbuRahma AF, Richmond BK, Robinson PA, Khan S, Pollack JA, Alberts S. Effect of contralateral severe stenosis or carotid occlusion on duplex criteria of ipsilateral stenoses: comparative study of various duplex parameters. J Vasc Surg 1995;22:751-61; discussion:761-2.

43. Spadone DP, Barkmeier LD, Hodgson KJ, Ramsey DE, Sumner DS. Contralateral internal carotid artery stenosis or occlusion: pitfall of correct ipsilateral classification–a study performed with color-flow imaging. J Vasc Surg 1990;11:642-9.

44. Henderson RD, Steinman DA, Eliasziw M, Barnett HJ. Effect of contralateral carotid artery stenosis on carotid ultrasound velocity measurements. Stroke 2000;31:2636-40.

45. Tang D, Teng Z, Canton G, Yang C, Ferguson M, Huang X, et al. Sites of rupture in human atherosclerotic carotid plaques are associated with high structural stresses: an in vivo MRI-based 3D fluid-structure interaction study. Stroke 2009;40:3258-63.

46. Li MX, Beech-Brandt JJ, John LR, Hoskins PR, Easson WJ. Numerical analysis of pulsatile blood flow and vessel wall mechanics in different degrees of stenoses. J Biomech 2007;40:3715-24.

47. Moneta GL, Edwards JM, Papanicolaou G, Hatsukami T, Taylor LM Jr, Strandness DE Jr, et al. Screening for asymptomatic internal carotid artery stenosis: duplex criteria for discriminating 60% to 99% stenosis. J Vasc Surg 1995;21:989-94.